C. R. Mecanique 338 (2010) 615–626

Contents lists available at ScienceDirect

Comptes Rendus Mecanique

www.sciencedirect.com

Micromechanics of granular materials

Modelling of volume change in granular materials in relation to their internal state

Modélisation des variations volumiques dans les matériaux granulaires prenant en compte leur état interne

Eric Vincens *, Yuhanis Yunus, Bernard Cambou

Université de Lyon, LTDS, UMR CNRS 5513, École centrale de Lyon, 36, avenue Guy-de-Collongue, 69134 Écully cedex, France

ARTICLE INFO

Article history:
Available online 20 October 2010

Keywords:
Granular media
DEM
Anisotropy
Characteristic state
Cycle
Hardening

Mots-clés :
Milieux granulaires
MED
Anisotropie
État caractéristique
Cycle
Écrouissage

ABSTRACT

Numerical simulations on samples composed of rigid spheres have been performed to study the behaviour of granular materials under complex stress paths involving peculiar triaxial monotonous stress paths and two-way cycling loading paths. These simulations using the Discrete Element Method (DEM), pointed out the concomitant role played by the void ratio and the anisotropy of fabric in the behaviour of these samples. Thus, the void ratio and the anisotropy of fabric have been chosen as internal variables for the description of the internal state of the material. An elastic-plastic model for soils, CJS, has been used to study the evolution of the material at the global scale. This work shows the complex path followed by some variables or key parameters involved in this model throughout simulations. Moreover, the parameters that are usually taken as constants in the CJS model definitely need to evolve with respect to the two internal variables in order to provide a precise prediction of the behaviour of granular materials throughout complex loadings.

RÉSUMÉ

Des essais numériques ont été réalisés sur des échantillons composés de sphères rigides pour étudier le comportement des matériaux granulaires sur des chemins de chargement complexes, impliquant des chemins triaxiaux monotones ou cycliques alternés. Ces simulations, qui utilisent la Méthode aux Eléments Discrets (MED), mettent en relief le rôle concomitant de l'indice des vides et de l'anisotropie de structure dans le comportement de ces échantillons. Aussi, l'indice des vides et l'anisotropie de structure ont-ils été choisis comme variables pour décrire le comportement de l'état interne du matériau. Par la suite, un modèle élastoplastique de sols, CJS, a été utilisé pour étudier l'évolution du matériau à l'échelle de l'échantillon. Ce travail montre le chemin complexe suivi par certaines variables ou paramètres de modèle impliqués dans CJS au cours de ces simulations. Les simulations ont établi que ces paramètres de modèle, généralement des constantes dans CJS, doivent être modifiés selon la valeur des deux variables internes identifiées afin d'obtenir une description plus fine du comportement des matériaux granulaires sur des chemins de contraintes complexes.

* Corresponding author.
E-mail address: eric.vincens@ec-lyon.fr (E. Vincens).

1631-0721/$ – see front matter
doi:10.1016/j.crme.2010.10.002

1. Introduction

So far, constitutive modelling of granular materials remains an open problem. Recently, even if compact and efficient phenomenological models were proposed to model the behaviour of soils [1–4] under monotonous loadings, accurate forecasts for granular soils submitted to complex loading paths are difficult to obtain. These difficulties arise from the lack of precise information about the evolution of the internal structure of granular soils. To overcome these difficulties, discrete element modelling (DEM) of granular materials can be very helpful. Indeed this method allows having access to information at both the local and sample scale while the conditions of the tests are precisely controlled. First, the DEM has been used as a substitute to experimental tests and as a convenient tool to analyse the global behaviour of granular materials in relation to different loading conditions or physical properties for the studied samples ([5–10], among others). Other authors have also used the DEM to reassess the general framework of elastoplasticity for granular material [11–13] and finally others have used this method to study the evolution of physical internal local variables all along different loading paths able to help to the improvement of constitutive modelling for soils [14–19].

This study is motivated by the latter aspect and DEM simulations of triaxial tests of different kinds were performed by Yunus [18] to investigate the evolution of the internal state of samples composed of polydisperse spheres throughout monotonous and cyclic loading paths. Different tests, involving different densities and different states of anisotropy, showed the dependency of classical reference states with the density and the anisotropy of fabric (orientation of normals at contact) [19]. These reference states are the state of maximum shear resistance and the characteristic state, transitory state between volumetric contractive deformations to dilative volumetric deformations for the granular material when shearing takes place. Thus, these two variables, void ratio and anisotropy of fabric, seem to be relevant to reflect the internal state of the material when loading [19].

The goal of this article is to show how some variables or parameters involved in the phenomenological model CJS [20,21] are related to the evolution of the two considered internal variables. This aspect was not addressed in previous works and typically shows the benefit of the approach to improve the forecast of constitutive models for soils. In particular, it tends to demonstrate that the parameters of constitutive models for soils must not be kept constant to provide a precise forecast of granular samples' behaviour. They must depend both on the void ratio and on the anisotropy of fabric.

First, the context of the simulations and some fundamental results obtained for the simulations performed from isotropic or anisotropic states will be recalled [19]. More precisely, we present the evolution of quantities measured at the sample scale throughout the performed triaxial simulations in relation with the internal state of the material. Secondly, the main equations of the constitutive model for soils, CJS, in relation with the studied variables or the model parameters are presented. Finally, equations relating these model parameters to both void ratio and anisotropy of fabric are presented and a forecast of the characteristic state using these models under a complex loading is compared to the one directly identified throughout numerical simulations.

2. Granular materials and construction of samples

The DEM simulations have been performed using PFC^{3D} software [22]. In this code, rigid spherical bodies with deformable contacts can be modelled. The law that rules the contact between two bodies is of Coulomb type and involves both a normal and a tangential stiffness (k_n and k_s respectively). It also requires the definition of a friction ratio f. Further dissipation in the system is included by means of a local non-viscous damping (also called Cundall's damping) α defined at the centre of each particle and proportional to acceleration forces.

The simulated material is composed of 10,000 spherical particles with diameters ranging from 3 cm to 6 cm. The procedure used for the sample construction has been accurately described in [19]. Three samples with different densities have been obtained using three different values for the friction ratio: 0.7, 0.4 and 0 for the densest sample. Hereafter, they will be denoted L50, M50 and D50. These friction ratios are imposed throughout the generation stage of the samples but are set to 0.7 throughout the simulated triaxial tests. Table 1 gives the values of all mechanical parameters considered in the numerical simulations.

Table 1
Mechanical properties of particles and walls.

Body	Mechanical properties	Values
Particles	Normal rigidity	1.0e7 (N/m^2)
	Tangential rigidity	1.0e7 (N/m^2)
	Friction ratio	0.70
	Damping coefficient	0.25
Walls	Normal rigidity	1.0e7 (N/m^2)
	Tangential rigidity	1.0e7 (N/m^2)
	Friction ratio	0.0

3. Numerical simulations

In this section we present the global trends obtained for some reference states such as the critical state, the state at maximum shear resistance and the characteristical state throughout simulations of monotonous triaxial tests. These simulations are performed from both isotropic and anisotropic initial states and involve samples having different initial densities.

3.1. Variables considered to characterise the internal state

Two variables have been considered to characterise the internal state: the void ratio e and a measure of the anisotropy of fabric, say the anisotropy of the orientation of normals at contacts. The tensor A associated to this anisotropy is derived from the fourth rank tensor defining the tensor of fabric H which is defined by [23]:

$$H_{ijkl} = \langle n_i n_j n_k n_l \rangle \tag{1}$$

where $\langle\,\rangle$ denotes the average over all the contacts. More details about the use of such fourth tensor and its relationship with the corresponding second order tensor of normals at contacts can be found in [18] or [24]. Then a tensor defining the anisotropy of fabric is defined as:

$$A_{ijkl} = H_{ijkl} - \frac{1}{3} tr(H_{ijkl}) \delta_{ijkl} \tag{2}$$

Due to the symmetry of the loading (triaxial tests) and for the sake of simplicity, the component A_{1111} will be taken as a measure of the anisotropy within the sample. It is clear that, for the kind of loading analysed in this paper, a second rank tensor would have given the same information. The fourth rank tensor has been chosen because it gives more accurate information in case of complex loadings [18,24] which will be considered in future studies.

3.2. Monotonous loadings from an isotropic initial state

Different triaxial tests have been performed on isotropically placed materials considering different initial densities and a confining stress of 50 kPa. Some main information obtained throughout the different simulations is drawn in Figs. 1(a), (c), for a compression stress path, and in Figs. 1(b), (d) for an extension path. In Fig. 1, the stress ratio q/p is the ratio between the second invariant of the stress tensor and the mean pressure. More complete results can be obtained in [19].

All the curves show that, for very large strains (axial strain larger than 30%), the sample reaches a unique state irrespective of the initial properties. This state corresponds to the well known "critical state" which is characterised by a critical stress ratio (q/p), a critical void ratio for a given confining pressure [25–27] and a critical anisotropy. One can note that the internal friction angle at the critical state obtained throughout a compression test and an extension test is different. This result has previously been well established from experimental results [28]. This discrepancy is also noticeable for the critical void ratio and the critical anisotropy obtained from a compression test and an extension test.

Fig. 2 shows the trends for the mobilised friction angle at maximum shear resistance state (peak state) and characteristic state. When increasing the density of the material, the internal friction angle at maximum shear resistance (peak) increases and the internal friction angle at characteristic state decreases. We recall that the characteristic state corresponds to a transitory state where the volumetric deformations pass from a contractive to a dilative pattern [29]. This result is in agreement with experimental results [30–32] and simulations performed on two-dimensional polygonal materials [33]. It implies that the dilative domain increases when the material is getting denser.

3.3. Monotonous loadings performed from anisotropic states

To have more insight onto the global behaviour of considered samples, further simulated triaxial tests have been performed on a sample exhibiting anisotropic initial states. In order to obtain an anisotropic state, sample L50 is first submitted to an extensive axial loading until reaching one of the following axial strains ε_1 of -2%, -5%, -10% or -45%, giving birth to four samples exhibiting distinct "initial" states of anisotropy (dark grey path in Figs. 3(a), (b), (c)). These four samples are subsequently and individually submitted to an axial loading in compression (stress reversal) performed up to an axial strain equal to 45% (pale grey paths in Figs. 3(a), (b), (c)).

Similar tests were performed in order to create an initial anisotropy in compression (compression test up to axial strains ε_1 of 2%, 5%, 10% or 45%), and from these states, extension tests are performed. They are not shown here.

Figs. 4(a) and (b) show the different values obtained for the internal friction angle at characteristic state, at maximum shear resistance (peak) and at critical state for these two series of simulations. As expected, the critical state is found independent of the "initial" anisotropy indicating that history has been totally erased by the large deformations. This is not the case for the peak state and the characteristic state. The peculiar shape of the curve related to the friction angle at characteristic state tends to show its dependency both on void ratio and anisotropy. Indeed, considering in Fig. 4(b) the results for the compression tests shown in Figs. 3(a), (b), (c), one can note that the friction angles at the characteristic state

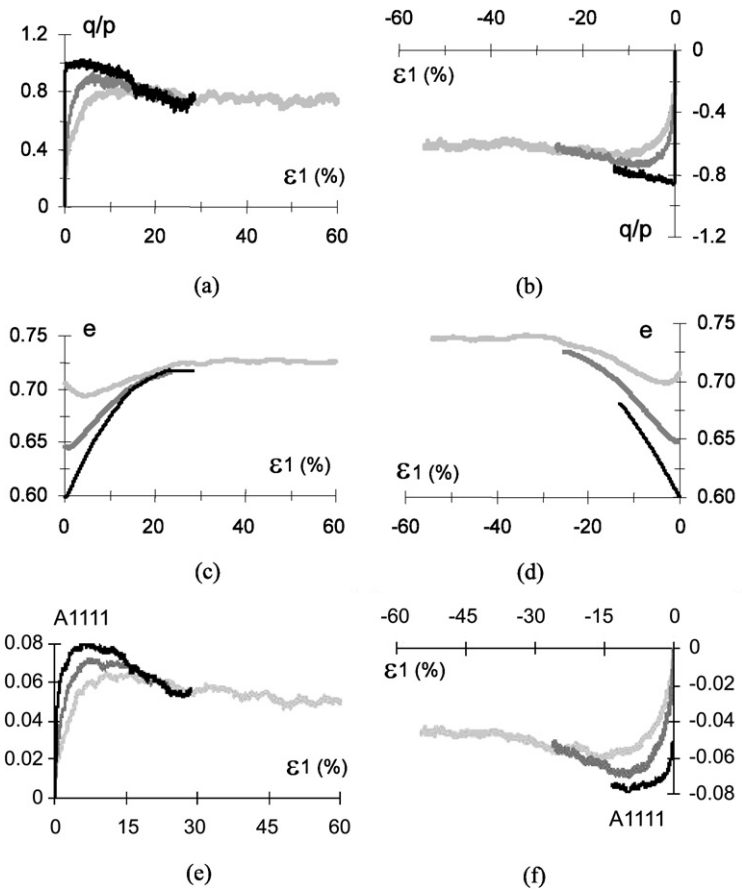

Fig. 1. Monotonous tests from isotropic states for samples: L50, M50, D50. (a), (c) Stress ratio and void ratio for a compression loading path respectively. (b), (d) Stress ratio and void ratio for an extension loading path respectively. (e), (f) Evolution of the anisotropy measure A_{1111}.

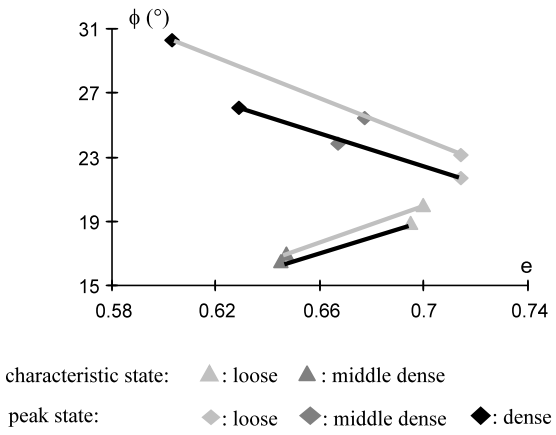

Fig. 2. Trends for the mobilised friction angle at characteristic state and at peak according to initial void ratio for sample L50: extension path, compression path.

evolve in a global similar way as the value of the void ratio at the "initial state": the angle decreases if the void ratio at the "initial state" decreases. But the void ratio at "initial state" for the test performed from ε_1 of -10% is greater than the void ratio corresponding to tests performed from ε_1 of 0%, -2% or -5%, though its friction angle at characteristic state is lower than the ones obtained for these latter tests. The same findings could be pointed out for the tests performed from ε_1 of -45%.

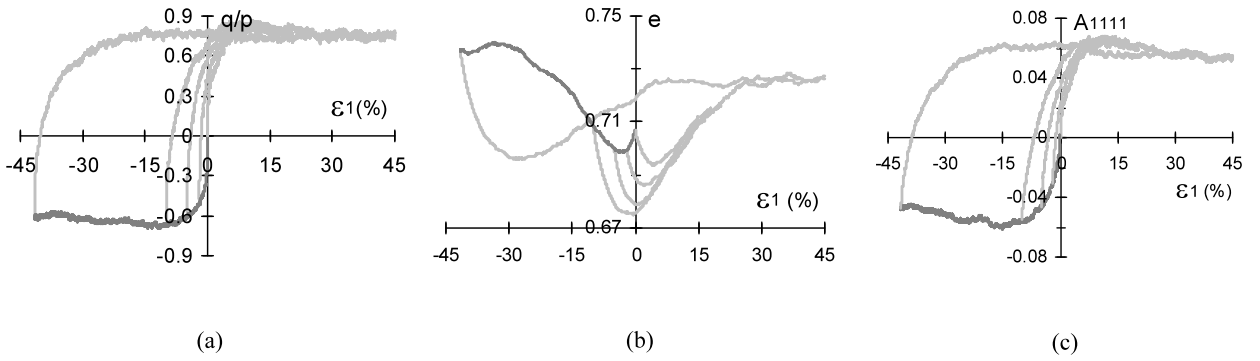

Fig. 3. Compression tests performed from different anisotropic initial states for sample L50: (a) stress ratio, (b) void ratio, (c) anisotropy measure A_{1111}.

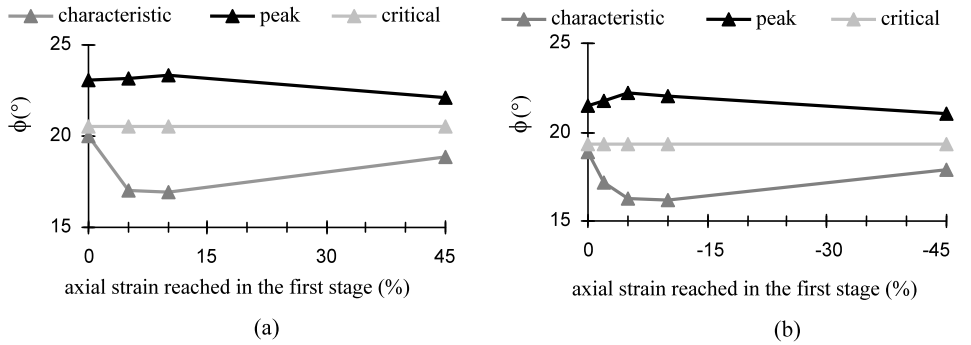

Fig. 4. Evolution of the mobilised friction angle at characteristic state, at peak and at critical state for sample L50: (a) extension test, (b) compression test.

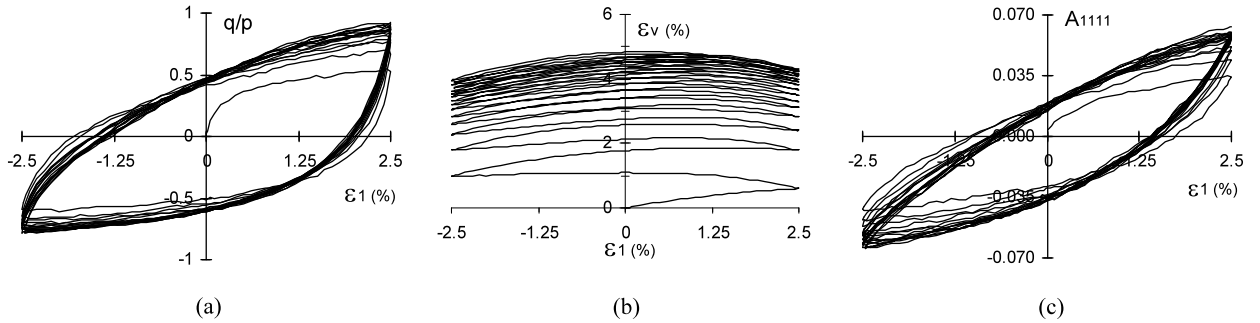

Fig. 5. Two-way cyclic loadings with axial strain amplitude of 2.5% for sample L50: (a) stress–strain curve, (b) volume strain evolution, (c) anisotropy evolution.

This demonstrates the necessary influence of a factor other than density. As the anisotropy of fabric tends to increase when the axial strain reached in the first stage increases, it seems to be responsible for damping out the influence of the void ratio at characteristic state. A same conclusion can be drawn for the friction angle at maximum shear resistance.

3.4. Cyclic loadings

Apart from monotonous tests, two-way cyclic triaxial loadings including 15 cycles of 2.5% axial strain amplitude were also performed on sample L50. These simulations were performed on a sample having an initial isotropic state. Figs. 5(a), (b), (c) present the results of the simulations showing in particular the evolution of the two internal variables considered in this paper: e (linked to ε_v) and A_{1111}. These tests will be analysed hereafter.

4. Presentation of CJS model

The CJS model is a phenomenological elastic-plastic model which has first been developed in 1989 [20] and improved later by Maleki [21].

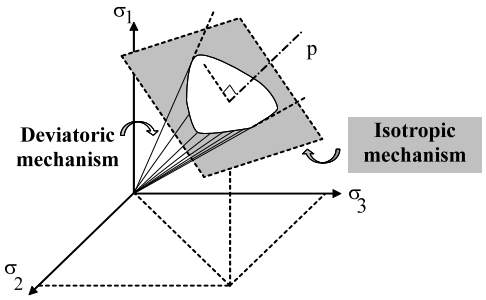

Fig. 6. Definition of the yield surfaces linked to the two mechanisms of plastic strains in CJS model.

The model takes into account two plastic strain mechanisms: one is related to the evolution of the isotropic part of the stress tensor, the other to the evolution of the deviatoric part of the stress tensor.

We will focus this short presentation on the latter mechanism which is described in the principal stress axes by a cone presented in Fig. 6. The evolution of this yield surface is ruled by two hardening mechanisms, an isotropic hardening which controls the spread angle (measured by the mean radius R in the deviatoric plane) of this cone and a kinematic hardening which controls the position of its axis (defined by the non-dimensional tensor X_{ij}).

The modelling of the plastic strain linked to the deviatoric mechanism of plasticity is defined from two usual equations: the first one defines the yield surface itself and the second one defines the plastic flow rule.

The yield surface which has the same shape as the isotropic failure surface is written:

$$f(\sigma_{ij}, R, X_{ij}) = q_{II} h(\theta) - R I_1 \tag{3}$$

with

$$q_{II} = (q_{ij} q_{ij})^{1/2}$$

$$q_{ij} = s_{ij} - X_{ij}.I_1$$

s_{ij} is the deviatoric part of the stress tensor, while I_1 is the first invariant of the stress tensor, θ is the Lode angle in the deviatoric plane and $h(\theta) = (1 - \gamma \cos 3\theta)^{1/6}$. γ is related to the dissymmetry of the yield surface which is stated to be equal to the dissymmetry of the isotropic failure surface.

The plastic flow rule is written:

$$\dot{\varepsilon}_v^{dp} = \beta \left(\frac{s_{II}}{s_{II}^{char}} - 1 \right) \frac{|s_{ij} \dot{\varepsilon}_{ij}|}{s_{II}} \tag{4}$$

where $\dot{\varepsilon}_{ij}$ is the increment of the strain tensor and s_{II} is the second invariant of the stress tensor. The value for s_{II}^{char} in Eq. (4) is obtained by stating the equation for the isotropic characteristic surface which defines the boundary between the contractancy and the dilatancy domains in the stress space:

$$f\left(\sigma_{ij}^{char}, R_{char}\right) = s_{II}^{char} h(\theta) - R_{char} I_1 \tag{5}$$

The characteristic surface separates the stress space into two domains, the inner space where only contractive volumetric deformations can take place and an outer domain where dilatancy is generated. For simplicity, this surface is generally supposed to be isotropic and herein it is defined by an average radius equal to R_{char} in the deviatoric plane. Some preliminary studies [18] have shown that the dissymmetry of this surface is actually different than the one observed for the failure surface and will be characterised by a specific γ value: γ_{char} in this study.

5. Evolution of some parameters used in CJS model with the internal state

The numerical simulations based on the DEM method give access to different types of information: first, information related to the internal state (through e and A_{1111}) and secondly to the evolution of some variables or parameters used in model CJS such as X_{II}, R, β, R_{char} and γ_{char} with respect to the internal state. The scalar X_{II} associated to the stress anisotropy is defined the same way as q_{II} was previously defined.

A first study involving the anisotropy X_{II} has been performed based on the analysis of the cyclic simulations described in Fig. 5. Figs. 7(a) and 8(a) present the path of this variable throughout the compression stages and extension stages of the two-way cycles respectively. Figs. 7(b) and 8(b) demonstrate that a close relationship exists between the anisotropy X_{II} and the anisotropy of normal at contacts which is a local anisotropy. The relation between X_{II} and A_{1111} seems to be linear in a first approximation for the stress path considered in this work.

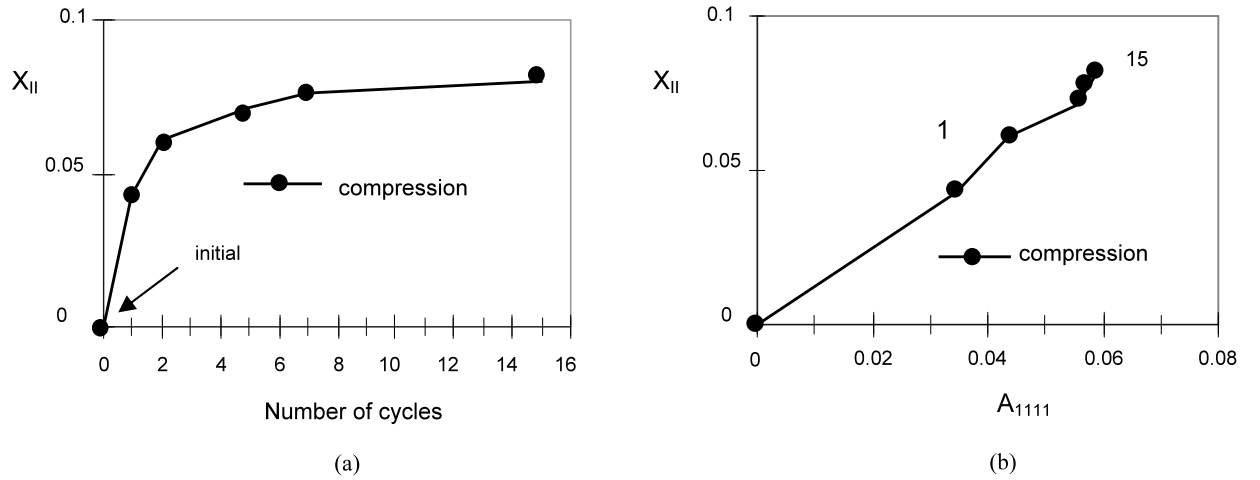

Fig. 7. Evolution of the anisotropy X_{II} throughout the compression stages of two-way cyclic loadings ($\varepsilon_1 = 2.5\%$): (a) against the number of cycles of loading, (b) against the local anisotropy measure A_{1111}.

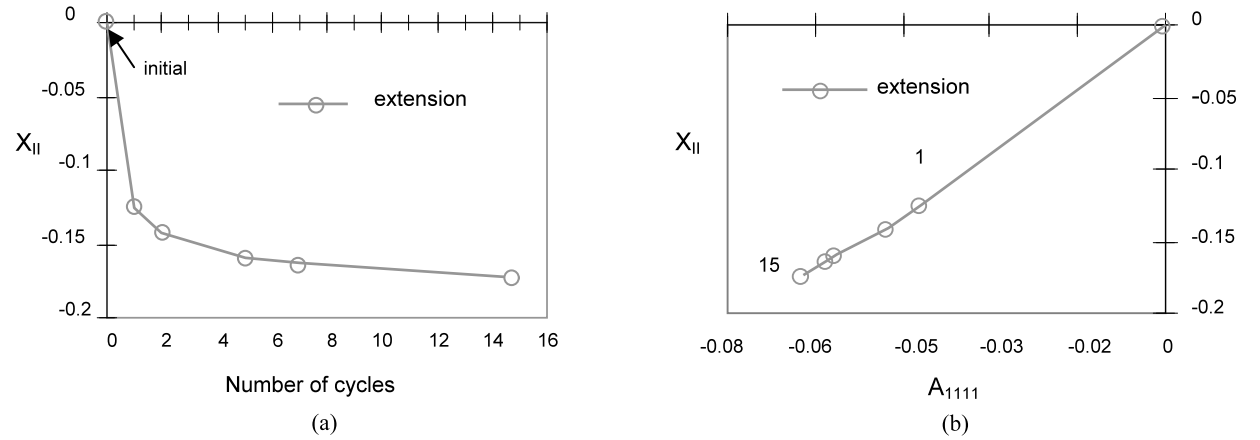

Fig. 8. Evolution of the anisotropy X_{II} throughout the extension stages of two-way cyclic loadings ($\varepsilon_1 = 2.5\%$): (a) against the number of cycles of loading, (b) against the local anisotropy measure A_{1111}.

The evolution of the elastic radius R of the deviatoric yield surface is given in Fig. 9(a) throughout both the compression and extension stages. The methodology used to obtain the different values for R is precisely explained in [19]. To identify R, we identify throughout the cycles the corresponding state of stress (second invariant of the stress tensor) when the dissipated energy from sliding at contacts in DEM starts to rise significantly. It signifies that, at this point, the irreversibilities within the sample become significant. R can only be identified when a reversal of loading direction takes place and is associated to the domain limited by the stress point mentioned before, and the maximum value of the second invariant of the stress tensor at reversal of loading.

The evolution for R is quite different throughout the stages of cycling and depends on the stress path. For the compression stages, a clear link between R and e can be identified, but this result seems to be more difficult to propose for the extension stages. This difficulty may arise from the hypothesis of considering γ as a constant throughout the cyclic loading.

A second analysis, involving the parameters defining the flow rule, say R_{char}, γ_{char}, β has been performed. For this, the two series of numerical simulations corresponding to monotonous loading applied on sample with an anisotropic "initial state", as presented in Fig. 3, have been used first. For convenience, we introduce normalised values for the internal variables e and A_{1111} defined by:

$$A_{nor} = \frac{A_{1111}^{cr} - A_{1111}^{ini}}{A_{1111}^{cr}} \quad \text{and} \quad e_{nor} = \frac{e^{cr} - e^{ini}}{e^{min} - e^{cr}} \tag{6}$$

The superscript *cr* stands for a value computed at the critical state, *ini* at the "initial state" (beginning of a stage of compression or extension throughout cycles) and e^{min} is the minimum void ratio for the material.

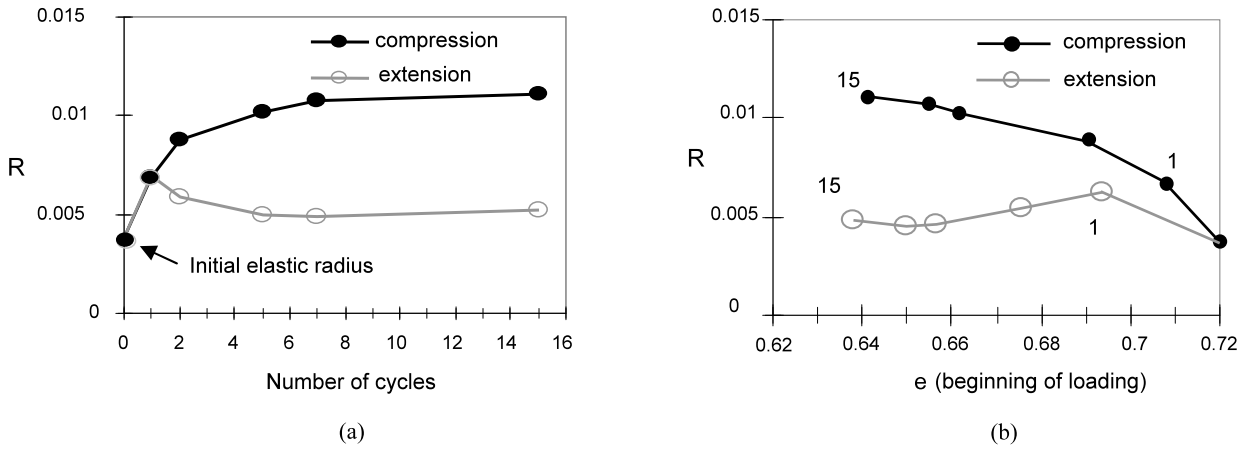

Fig. 9. Evolution of the elastic radius of the deviatoric yield surface throughout compression and extension stages of two-way cyclic loadings ($\varepsilon_1 = 2.5\%$): (a) against the number of cycles of loading, (b) against the void ratio at the beginning of each stage.

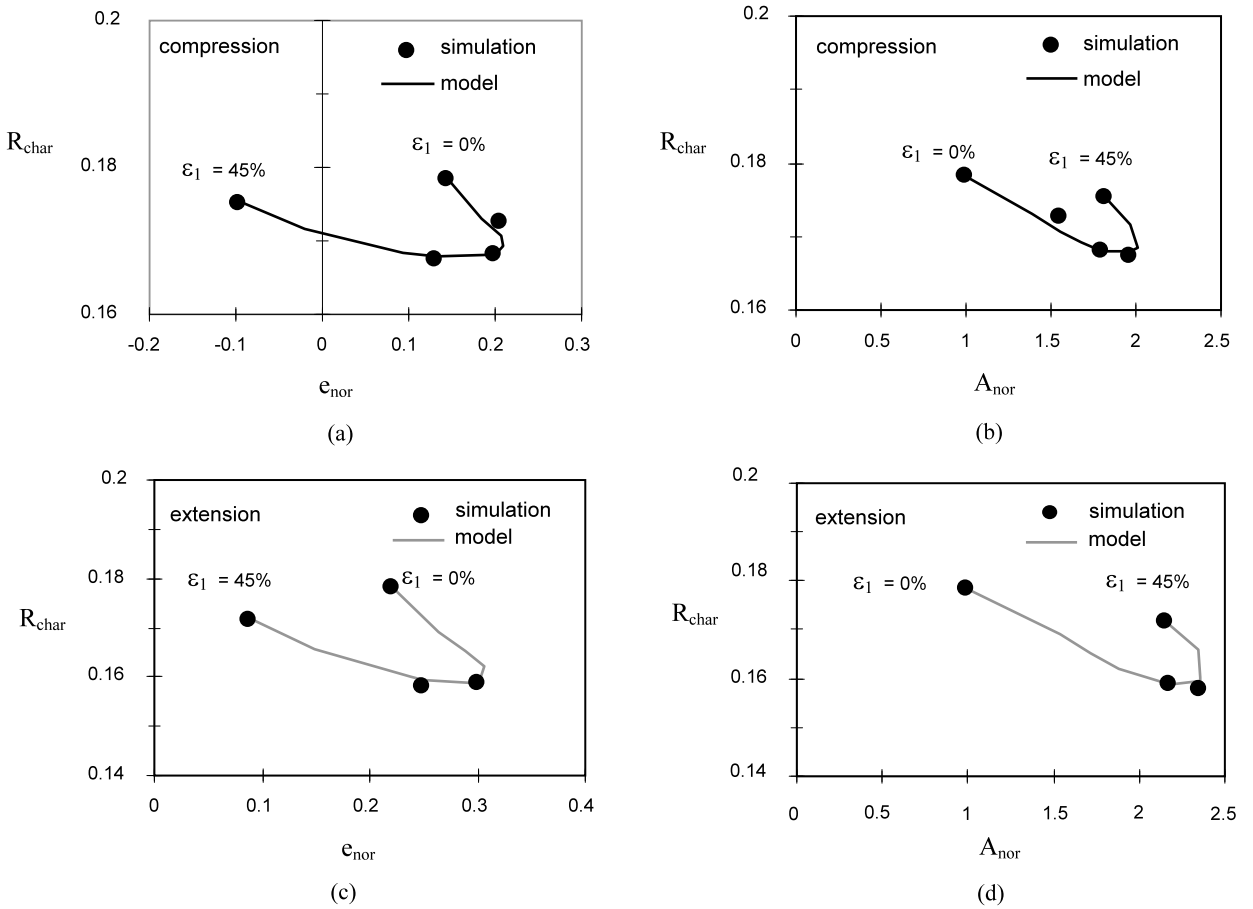

Fig. 10. Evolution of the radius of the isotropic characteristic surface throughout different loadings performed from different initial states corresponding to an initial value for the axial strain: (a), (b) compression stress path, (c), (d) extension stress path.

The results are depicted in Figs. 10(a)–(d), 11(a)–(d) and 12(a)–(d) with bullets. They show that the parameters R_{char}, γ_{char}, β depend not only on an isotropic internal variable e_{nor} but also on an internal variable related to the anisotropy A_{nor}. This aspect is never taken into account in usual constitutive model for soils.

Then, a bilinear relationship is introduced to relate the model parameters with the internal normalised variables:

$$\beta = B_0 - \psi|A_{nor}| + \xi(e_{nor}) \tag{7}$$

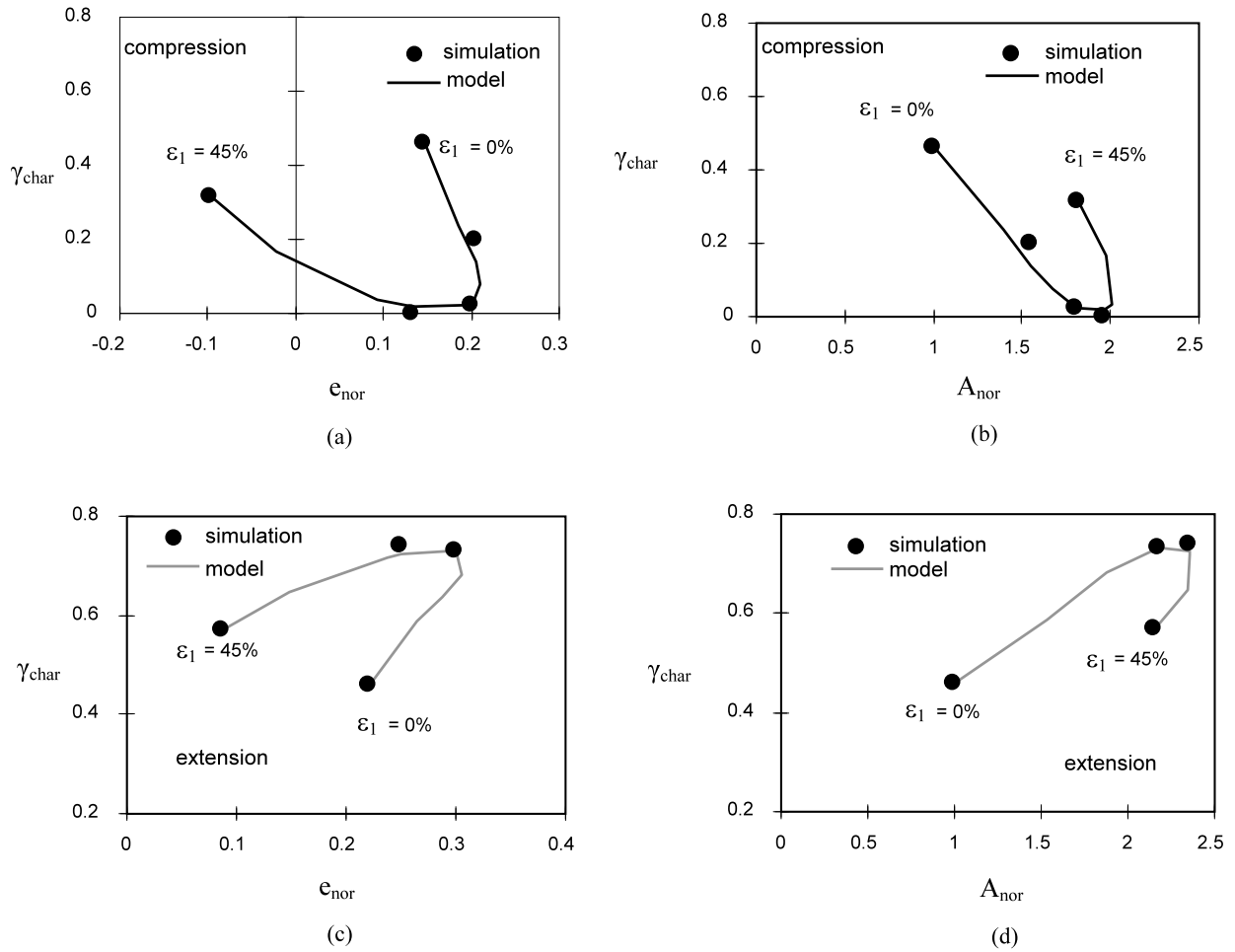

Fig. 11. Evolution of the dissymmetry of the isotropic characteristic surface throughout different loadings performed from different initial states corresponding to an initial value for the axial strain: (a), (b) compression stress path, (c), (d) extension stress path.

$$\gamma_{char} = C_0 - \eta|A_{nor}| + \lambda(e_{nor}) \tag{8}$$

$$R_{char} = D_0 - \delta|A_{nor}| + \tau(e_{nor}) \tag{9}$$

with parameters B_0, ψ, ξ, C_0, η, λ, D_0, δ, τ for the relationships. The result given by the bilinear relationships (model) is also depicted in Figs. 10(a)–(d), 11(a)–(d) and 12(a)–(d).

The set of parameters involved in Eqs. (7), (8) and (9) is identified throughout the compression and extension stress paths of the tests performed from different anisotropic states mentioned in Section 3.2. Nevertheless, since different quantitative patterns were obtained according to the stress path, two sets of parameters were settled, one for a compression stress path and one for the extension stress path. The values for these parameters can be found in Tables 2, 3 and 4 for the model parameters β, γ_{char} and R_{char} respectively. It tends to demonstrate that the behaviour of granular soils in compression or extension paths is quite different. This feature is generally not addressed in the usual constitutive model for granular soil (apart from the introduction of parameter γ related to the dissymmetry of the failure surface in the deviatoric plane).

The models defined by Eqs. (7), (8) and (9) have then been used to define the value for the stress ratio q/p at the characteristic state q/p_{char} for a different stress path than the one used for the identification of the parameters. For this purpose, the 15 two-way cyclic loadings presented in Fig. 5 are considered. The forecast obtained is drawn in Figs. 13(a), (b) and compared with the values directly identified throughout the cyclic simulations. The prediction obtained here is very good and provides a first validation of the models defined here above. The values of the stress ratio for the characteristic state obtained by the default process in the CJS model are also given in Figs. 13(a) and (b). In the CJS model, the characteristic state is not likely to evolve and q/p_{char} is kept constant throughout the cycles but different in compression and extension. Generally, the value in compression is identified by a monotonous compression triaxial test (sample supposed to be in an initial isotropic state). For simplicity, the corresponding value in extension is generally not identified by means of a monotonous extension test but can be deduced from the CJS model considering that the dissymmetry of the characteristic surface γ_{char} is equal to that of the failure surface γ. Guided by this usual identification process, q/p_{char} was found equal to

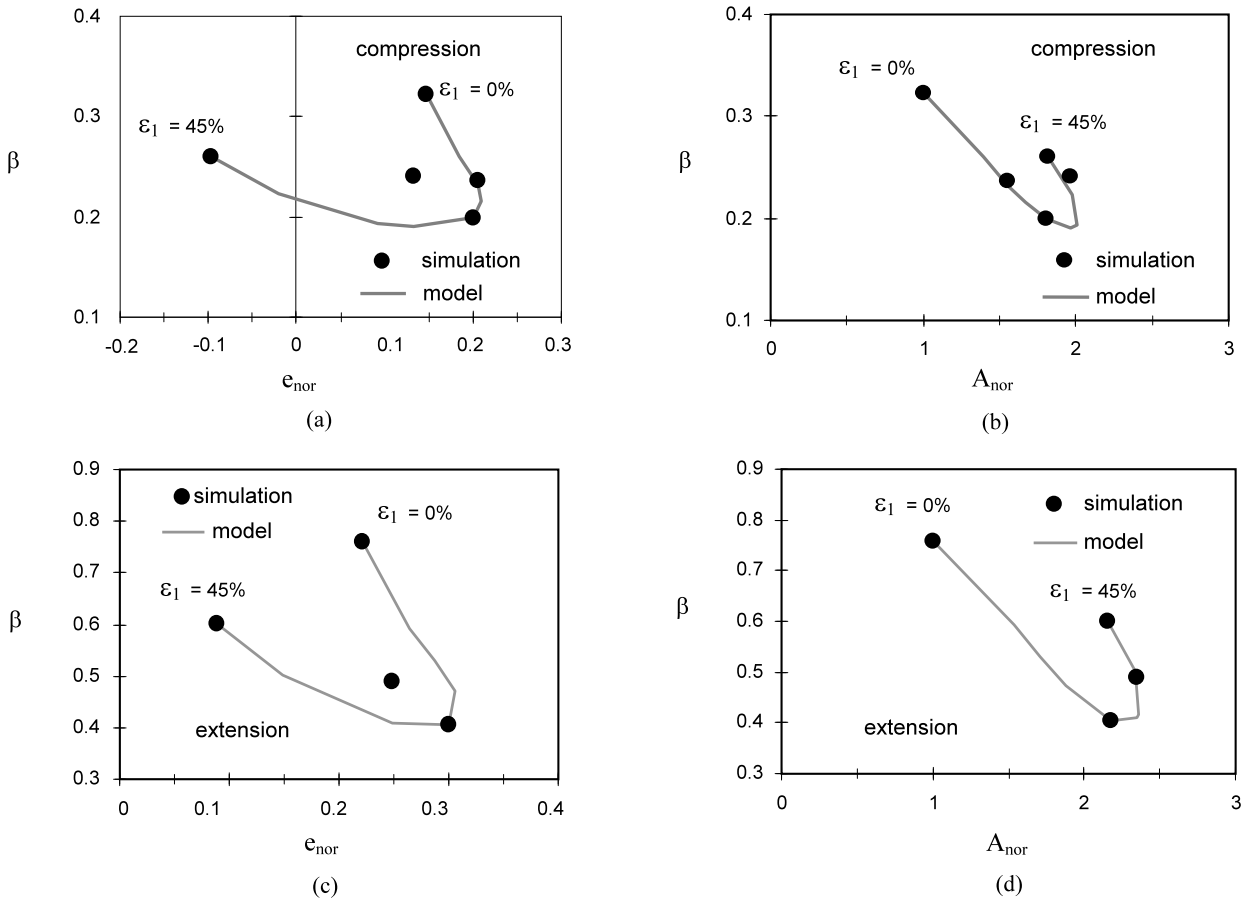

Fig. 12. Evolution of the parameter β involved in the flow rule associated to the deviatoric plastic mechanism throughout different loadings performed from different initial states corresponding to an initial value for the axial strain: (a), (b) compression stress path, (c), (d) extension stress path.

Table 2
Values of the parameters related to the bilinear model for β.

Parameters	Compression	Extension
B_0	0.4940	1.1977
ξ	−0.2133	−0.8973
ψ	0.1398	0.2401

Table 3
Values of the parameters related to the bilinear model for γ_{char}.

Parameters	Compression	Extension
C_0	1.0823	0.1151
λ	−1.0116	0.7435
η	0.4740	−0.1805

0.726 for L50. Indeed, since both extension and compression tests are available, γ can be computed stating that both stress states at peak in compression and extension belong to the same failure surface written as:

$$f\left(\sigma_{ij}^{fail}, R_{fail}\right) = s_{II}h(\theta) - R_{fail}I_1 \tag{10}$$

with s_{II} the second invariant of the stress tensor written at maximum shear resistance (failure), and R_{fail} the isotropic mean radius of the failure surface, $h(\theta) = (1 - \gamma\cos 3\theta)^{1/6}$ and θ is the Lode angle in the deviatoric plane. Then, γ is derived from the ratio:

$$\frac{(\frac{s_{II}}{I_1})_{ext}^{fail}}{(\frac{s_{II}}{I_1})_{comp}^{fail}} = \frac{(1-\gamma)^{1/6}}{(1+\gamma)^{1/6}} \tag{11}$$

Table 4
Values of the parameters related to the bilinear model for R_{char}.

Parameters	Compression	Extension
D_0	0.1929	0.2042
τ	−0.0249	−0.0601
δ	0.0110	0.0126

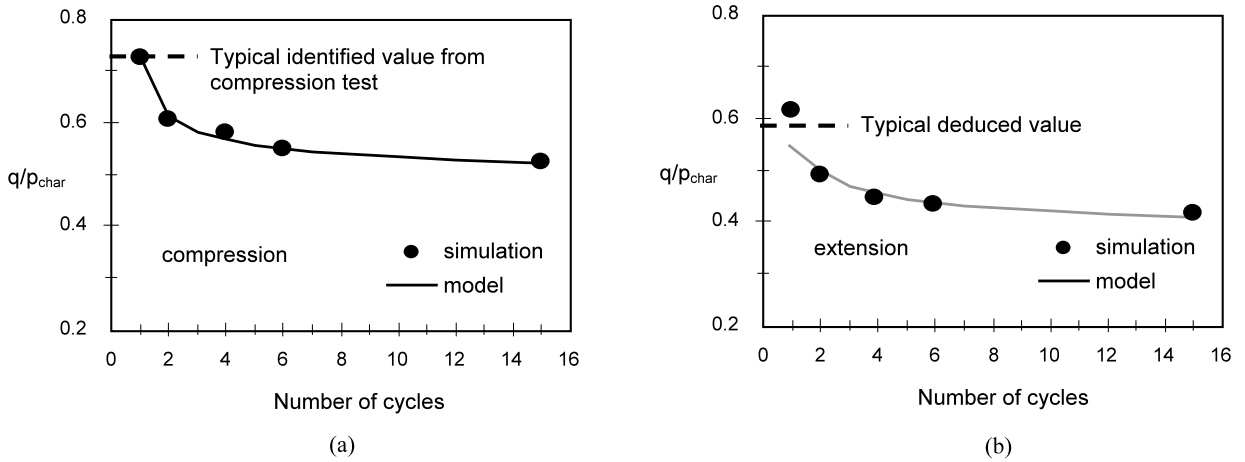

Fig. 13. Predictive model for the value of the stress ratio at the characteristic state throughout two-way cyclic loadings and typical values identified in classical version of CJS: (a) compression stage, (b) extension stage.

For L50, γ was found equal to 0.54. Then, since it was stated that the characteristic surface has the same dissymmetry as the failure surface:

$$\frac{(\frac{q}{p})^{char}_{ext}}{(\frac{q}{p})^{char}_{comp}} = \frac{(1-\gamma)^{1/6}}{(1+\gamma)^{1/6}} \tag{12}$$

so q/p_{char} in extension is equal to 0.594.

One can note the benefits from taking into account of both the void ratio and the anisotropy (Eqs. (7), (8), (9)) in order to model the decreasing value of the stress ratio at characteristic state throughout cycles. Nevertheless, one can also note that it was obtained with numerous parameters and further studies are required in order to relate them to values obtained for example at the critical state, state which is peculiar since being unique for a granular material. Moreover, the aim of further work will be to propose a method giving the access to the local anisotropy by means of a measure of quantities at the sample scale.

6. Conclusions

Numerical simulations of monotonous and two-way cyclic triaxial tests were performed on a granular material composed of spheres. Different reference states were derived from these simulations: the characteristic state, the state at maximum shear resistance and the critical state. The first two states were found strongly dependent on the internal state of the material, that is to say, the void ratio and the anisotropy of normals at contacts. Some relationships were drawn between some variables involved in the constitutive model for granular soil CJS and the evolution of the internal state of the granular material. The variable related to anisotropy in this model was then found closely related to the local anisotropy. The simulations show also that the parameters involved in the CJS model depend not only on the void ratio but also on the anisotropy of the material. Bilinear relationships were designed to correlate some key parameters associated to the flow rule of the deviatoric plastic mechanism to the internal state. Their relevancy was established but further study is required to stress the identification of the parameters and to provide a measure of the local anisotropy by a measure of quantities at the sample scale.

References

[1] X.S. Li, A sand model with state dependent parameter, Géotechnique 52 (3) (2002) 173–186.
[2] H.L. Fang, A state dependent multi-mechanism model for sands, Géotechnique 53 (4) (2003) 407–420.
[3] J. Yang, X.S. Li, State-dependent strength of sands from the perspective of unified modelling, Journal of Geotechnical and Geoenvironmental Engineering 130 (2) (2004) 186–198.

[4] C.S. Chang, P.Y. Hicher, An elasto-plastic model for granular materials with microstructural consideration, International Journal of Solids and Structures 42 (2005) 4258–4277.
[5] A.A. Mirghasemi, L. Rothenburg, E.L. Matyas, Numerical simulations of assemblies of two-dimensional polygon-shaped particles and effects of confining pressure on shear strains, Soils and Foundations 37 (3) (1997) 43–52.
[6] F. Radjai, D.E. Wolf, Features of static pressure in dense granular media, Granular Matter 1 (1) (1998) 3–8.
[7] C. Thornton, Numerical simulations of deviatoric shear deformation of granular media, Géotechnique 50 (1) (2000) 43–53.
[8] A.A. Mirghasemi, L. Rothenburg, E.L. Matyas, Influence of particle shape on engineering properties of assemblies of two-dimensional polygon-shaped particles, Géotechnique 52 (3) (2002) 209–217.
[9] C. Nouguier-Lehon, B. Cambou, E. Vincens, Structural changes in granular materials: The case of irregular polygonal particles, International Journal of Solids and Structures 42 (24–25) (2005) 6356–6375.
[10] C. Salot, P. Gotteland, P. Villard, Influence of relative density on granular materials behavior: DEM simulations of triaxial tests, Granular Matter 11 (2009) 221–236.
[11] F. Alonso-Marroquin, S. Luding, H.J. Herrmann, I. Vardoulakis, Role of anisotropy in the elastoplastic response of a polygonal packing, Physical Review E 71 (2005) 051304.
[12] C. Tamagnini, F. Calvetti, G. Viggiani, An assessment of plasticity theories for modeling the incrementally nonlinear behavior of granular soils, Journal of Engineering Mathematics 52 (2005) 265–291.
[13] F. Froiio, J.-N. Roux, An assessment of plasticity theories for modeling the incrementally non-linear behavior of granular soils, in: J. Goddard, J.T. Jenkins, P. Giovine (Eds.), IUTAM-ISIMM Symposium on Mathematical Modelling and Physical Instances of Granular Flows, 2010, pp. 183–197.
[14] L. Rothenburg, R.J. Bathurst, Analytical study of induced anisotropy in idealized granular materials, Géotechnique 39 (4) (1989) 601–614.
[15] N.P. Kruyt, Contact forces in anisotropic frictional granular materials, International Journal of Solids and Structures 40 (13–14) (2003) 3537–3556.
[16] M. Madadi, O. Tsoungui, M. Latzel, S. Luding, On the fabric tensor of polydisperse granular materials in 2D, International Journal of Solids and Structures 41 (2004) 2563–2580.
[17] T.T. Ng, Macro- and micro-behaviors of granular materials under different sample preparation methods and stress paths, International Journal of Solids and Structures 41 (2004) 5871–5884.
[18] Y. Yunus, Modélisation discrète du comportement cyclique des matériaux granulaires (in French), PhD, Ecole Centrale de Lyon, 2008.
[19] Y. Yunus, E. Vincens, B. Cambou, Numerical local analysis of relevant internal variables for constitutive modelling of granular materials, International Journal for Numerical and Analytical Methods in Geomechanics 34 (11) (2010) 1101–1123.
[20] B. Cambou, K. Jafari, A constitutive model for granular materials based on two plasticity mechanisms, in: Constitutive Equations for Granular Non-cohesive Soils, Saada & Bianchini, Balkema, Rotterdam, 1989, pp. 149–167.
[21] M. Maleki, B. Cambou, M. Farsi, P. Dubujet, An elastoplastic–viscoplastic model for soils. Numerical models in geomechanics, in: Proceedings of the 7th International Symposium, Graz, September 1999, pp. 15–20.
[22] P. Cundall, O. Strack, A discrete numerical model for granular assemblies, Géotechnique 29 (1979) 47–75.
[23] B. Cambou, F. Sidoroff, Distribution orientée dans un milieu granulaire et leurs représentations, in: Journées de mécanique aléatoire appliquée à la construction, éditions LCPC, 1986, pp. 199–204.
[24] J. Rahmoun, D. Kondo, O. Millet, A 3D fourth order fabric tensor approach of anisotropy in granular media, Computational Materials Science 46 (4) (2009) 869–880.
[25] A. Casagrande, Characteristics of cohesionless soils affecting the stability of slopes and earth fills, Journal of the Boston Society of Civil Engineering (January 1936) 13–32.
[26] K.H. Roscoe, A.N. Schofield, A. Thurairajah, Yielding of clays in states wetter than critical, Géotechnique 13 (3) (1963) 211–240.
[27] S.J. Poulos, The steady state of deformation, Journal of the Geoenvironmental Engineering Division ASCE 105 (2) (1981) 201–255.
[28] Y.P. Vaid, E.K.F. Chung, R.H. Kuerbis, Stress path and steady state, Canadian Geotechnical Journal 27 (1990) 1–7.
[29] M.P. Luong, Stress strain aspects of cohesionless soils under cyclic and transient loading, in: Proceedings of the International Symposium on Soils under Cyclic and Transient Loading, Swansea, 1980, pp. 353–376.
[30] D. Negussey, Vaid Y.P. Wijewickreme, Constant volume friction angle of granular materials, Canadian Geotechnical Journal 25 (1988) 50–55.
[31] B.S. Pradhan, F. Tatsuoka, On stress–dilatancy equations of sand subjected to cyclic loading, Soils and Foundations 29 (1) (1989) 65–81.
[32] H. Shahnazari, I. Towhata, Torsion shear tests on cyclic stress–dilatancy relationship of sand, Soils and Foundations 42 (1) (2002) 105–119.
[33] E. Vincens, C. Nouguier-Lehon, B. Cambou, Cyclic behavior of a two dimensional polygonal-shaped material, in: 16th ALERT Geomaterials Workshop, Aussois, October 10–12, 2005, http://alert.epfl.ch/Archive/ALERT2005/ALERTworkshop2005.html.